COMMUNICATION

Giant Photoamplification in Indirect-Bandgap Multilayer MoS_2 Phototransistors with Local Bottom-Gate Structures

Junyeon Kwon, Young Ki Hong, Gyuchull Han, Inturu Omkaram, Woong Choi, Sunkook Kim,* and Youngki Yoon**

Recently, there has been a growing interest in transition metal dichalcogenides, such as molybdenum disulfide (MoS_2), due to their intriguing electrical and optical properties.[1–9] Thin-film transistors (TFTs) using single layer or multilayer MoS_2 have shown promising switching behaviors including high on/off current ratio ($I_{on}/I_{off} \approx 10^8$), low subthreshold swing ($SS \approx 70$ mV decade^{-1}) and high field-effect mobility ($\mu_{eff} > 100$ cm^2 V^{-1} s^{-1}).[10–15] In addition, they also exhibited higher responsivity[16–19] than that of graphene TFTs in phototransistors,[20] presenting great potential for photodetector applications. The responsivity, defined as the ratio of photocurrent flowing in a detector to incident optical power, is a primary figure of merit in photodetectors. To enhance the responsivity of MoS_2 phototransistors, various approaches have been suggested including the improvement of mobility,[18] contact resistance,[18] and interfacial quality of MoS_2 phototransistors,[19] or the use of multijunction heterostructures with amorphous silicon[21] or graphene.[22,23] As a result, the responsivity of single layer MoS_2 phototransistors has been drastically increased from 7.5 mA W^{-1}[16] to 880 A W^{-1}.[18] Meanwhile, the responsivity of multilayer MoS_2 phototransistors (≈100 mA W^{-1})[17] has remained much lower than that of single layer MoS_2 photodevices, mainly due to the indirect nature of the bandgap in multilayer MoS_2.

In principle, multilayer MoS_2 can be more advantageous than single layer MoS_2 for a variety of photodetector applications due to the higher density-of-states[11] and the wider spectral response from ultraviolet (UV) to near-infrared (NIR).[17] Therefore, in this work, we focus on the optoelectronic design of multilayer MoS_2 phototransistors to enhance photocurrent and demonstrate an alternative approach to obtain high photoresponsivity using indirect-bandgap multilayer MoS_2. Unlike the previous multilayer MoS_2 phototransistors with global bottom-gate structures, our multilayer MoS_2 phototransistors are fabricated in a patterned local bottom-gate TFT configuration to achieve giant improvement in photoresponse. For the light with the wavelength of 532 nm, our phototransistor based on mechanically exfoliated MoS_2 flakes exhibits high responsivity (up to 342.6 A W^{-1} at 2 mW cm^{-1}) and linear relationship between photocurrent and incident power density over a wide range of optical power. In particular, the inclusion of ungated region in the MoS_2 channel increases responsivity by 3 orders of magnitude as compared to that of global-gate multilayer MoS_2 phototransistors from the previous study.[17] We further describe our experimental results with comprehensive simulations based on optical absorption, transmission probability, and transistor current equations.

Figure 1a shows the 3D section view of a phototransistor with a local bottom gate on a glass substrate. This phototransistor has a similar configuration to that of a commercially used bottom-gate inverted-staggered device. The typical structure contains gate metal underneath the active layer and source/drain contacts on the top. However, unlike the conventional structure, the gate length is shorter than the channel length as shown in the optical microscope image (Figure 1b). This "local" bottom-gate structure leads to a gate underlap, which is a non-overlapped (ungated) region between the gate and the channel (black area in the image). Figure 1c is the 3D atomic force microscope (AFM) image of the same device, which depicts the local bottom-gate structure more clearly. Figure 1d shows the AFM line scan profile (along the red line in Figure 1c) with a schematic diagram of the phototransistor, where gate underlap can be observed at both edges of the gate electrode. They can act like series resistors in dark state since gate modulation will be ineffective in the underlap regions.

Before analyzing the optoelectronic behavior of a multilayer MoS_2 phototransistor under incident light, we first measure current–voltage (I–V) characteristics of a local bottom-gate MoS_2 TFT (channel length $L \approx 11.2$ µm, device width $W \approx 31.0$ µm, and gate length ≈ 8.8 µm) in dark state. The thickness of multilayer MoS_2 channel and gate oxide thickness (t_{ox}) are 80 nm and 100 nm, respectively. **Figure 2**a shows the measured transfer ($I_{ds} - V_{gs}$) characteristics in logarithmic scale and the extracted mobility value of the TFT. The maximum transconductance $\left(g_m = \left.\frac{\partial I_{ds}}{\partial V_{gs}}\right|_{V_{ds}=1\,V}\right)$ of 4.38 µS, a field-effect mobility ($\mu_{eff} = Lg_m/(WC_{ox}V_{ds})$) of 25.55 cm^2 V^{-1} s^{-1}, and I_{on}/I_{off} of ≈10^3 are observed. Here, an atomic layer deposited aluminum oxide (Al_2O_3) gate insulator exhibits excellent insulating properties

J. Kwon, Dr. Y. K. Hong, Dr. I. Omkaram, Prof. S. Kim
Multi-Functional Nano/Bio Electronics Lab
Kyung Hee University
Gyeonggi 446-701, South Korea
E-mail: kimskcnt@gmail.com
G. Han, Prof. Y. Yoon
Department of Electrical and Computer Engineering
and Waterloo Institute for Nanotechnology (WIN)
University of Waterloo
Waterloo, ON N2L 3G1, Canada
E-mail: youngki.yoon@uwaterloo.ca
Prof. W. Choi
School of Advanced Materials Engineering
Kookmin University
Seoul 136-702, South Korea
E-mail: woongchoi@kookmin.ac.kr

DOI: 10.1002/adma.201404367

© 2015 WILEY-VCH Verlag GmbH & Co. KGaA, Weinheim

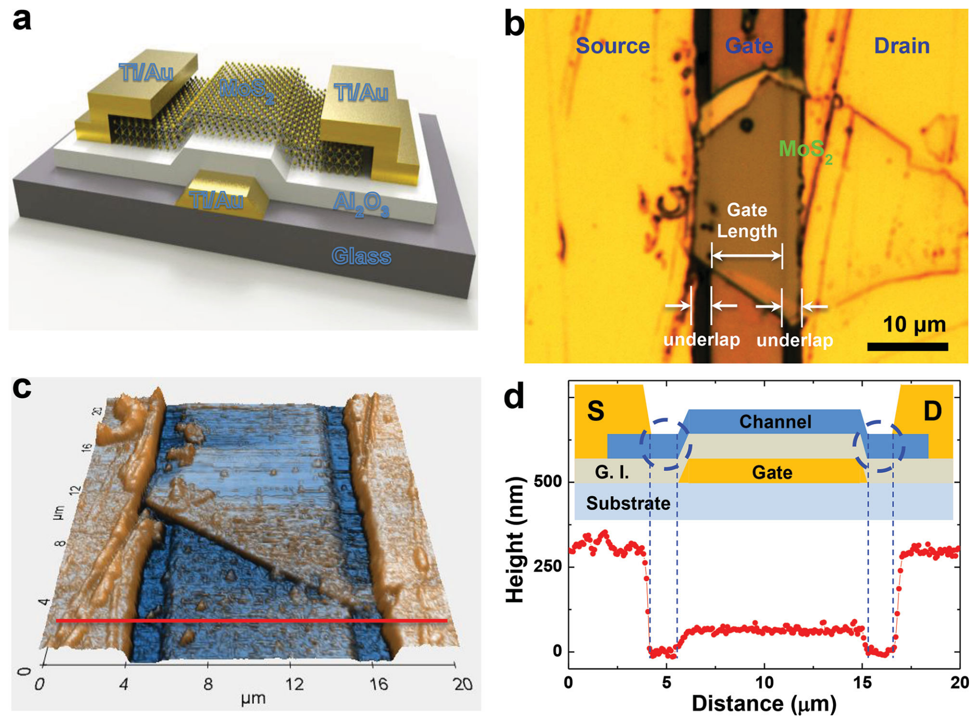

Figure 1. Multilayer MoS_2 phototransistor in a local bottom-gate structure. a) 3D schematic figure of a local bottom-gate MoS_2 phototransistor. b) Optical microscopy image and c) 3D AFM topographic image of the device, showing ungated MoS_2 channel regions (gate underlap) between the gate and the source/drain electrodes. d) Topological analysis of line profile data obtained along red line in Figure 1c. (Inset) Cross-sectional view of the device.

(leakage current = ≈50 pA at V_{gs} = 5 V) and offers well-controlled electrostatic potential with a relatively small gate-bias modulation. Figure 2b shows the output ($I_{ds} - V_{ds}$) characteristics of the same device. Titanium/gold (Ti/Au) source and drain electrodes provide excellent ohmic contacts to the multilayer MoS_2, resulting in the linear behavior at low drain voltages, and the fully saturated current at high V_{ds}. Although our local bottom-gate MoS_2 phototransistor shows the device characteristics of conventional *n*-type long-channel TFTs in dark state, its performance is not as good as that of other reported global-gate multilayer MoS_2 TFTs due to the underlap in the local-gate geometry.

In general, good contact properties are essential to ensure large drive current, especially for the transistors with significant gate underlap regions. We have estimated the degradation of current due to the gate underlap as:

$$I_{dark}^{local} = I_{dark}^{global} \times \overline{Tr}^{underlap} \quad (1)$$

where I_{dark}^{local} and I_{dark}^{global} are dark current for local-gate and global-gate structure, respectively, and $\overline{Tr}^{underlap}$, the average transmission probability through the underlap region, is introduced to consider current degradation due to the gate underlap. First, $I_{dark}^{global} = 3.00 \times 10^{-5}$ A is obtained from the current equation for the conventional long-channel devices in the linear region with the following parameters: field-effect mobility of 100 $cm^2\ V^{-1}\ s^{-1}$,[11] oxide capacitance of 6.20 × 10^{-4} F m^{-2}, device width of 31.0 μm, channel length of 11.2 μm at $V_{on} = V_{gs}$ = 6.5 V (threshold voltage, V_{th} = 4.75 V) and V_{ds} = 1 V. Since the measured current value of our local-gate device structure at the same bias condition (V_{gs} = 6.5 V and V_{ds} = 1 V with V_{th} = 4.75 V) is 3.31 × 10^{-6} A, we estimate $\overline{Tr}^{underlap}$ to be 0.11 and the current is smaller than that of an ideal global-gate TFT by roughly 1 order of magnitude. In order to understand this current degradation, we calculated transmission probability through the gate underlap at on state assuming two different contact conditions as shown in **Figure 3**a. First, we defined a relatively large Schottky barrier height (Φ_{Bn} = 100 meV) and calculated a transmission probability through the triangular tunnel barrier in the gate underlap region by varying the length of underlap from 1 Å to 1 μm (squares in Figure 3b). Our simulation result shows that transmission probability becomes zero at a 1-μm gate underlap, which clearly indicates that current cannot flow through the large Schottky barrier if the underlap length is significant as in our device (1.41 μm). Obviously, this is not the case that we have observed in our experiment. Next, we defined a small Schottky barrier (Φ_{Bn} = 10 meV) assuming that carrier transport is near-thermionic rather than tunneling as illustrated at the bottom in Figure 3a. The transmission probability is calculated again at the top of the barrier for the same range of gate underlap. Our result shows that, under this condition, the current decreases gradually as the underlap length increases, but will not be completely diminished even with 1-μm gate underlap. This indicates that a normal TFT operation is still possible with our local-gate structure even though current level will be reduced as compared to that of global-gate TFTs. Therefore, our analysis, along with the linear I_{ds}–V_{ds} behavior at low drain voltages, implies that the Schottky barrier height of our

© 2015 WILEY-VCH Verlag GmbH & Co. KGaA, Weinheim

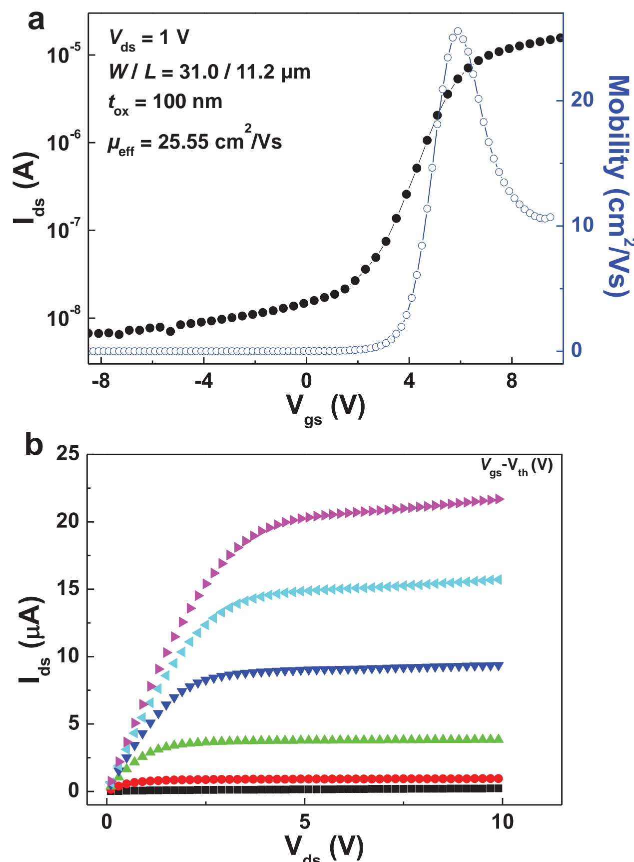

Figure 2. a) Transfer characteristic ($I_{ds} - V_{gs}$) curve and field-effect mobility of the local bottom-gate multilayer MoS_2 phototransistor at V_{ds} = 1 V. b) Output characteristic (I_{ds}–V_{ds}) curves of the same device with different gate biases ($V_{gs} - V_{th}$ = 4, 5, 6, 7, 8, and 9 V).

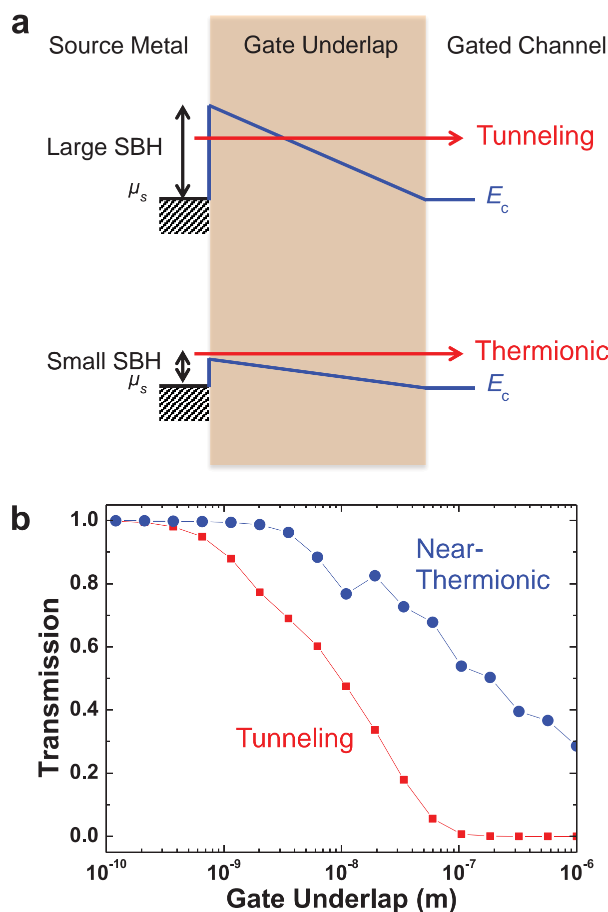

Figure 3. a) Tunneling (top) and near-thermionic emission (bottom) through the gate underlap with a large and a small Schottky barrier height (SBH), respectively, at the metal-MoS_2 interface. μ_s is the chemical potential at the source and E_c is the conduction band edge of MoS_2. b) Transmission probability at various lengths of gate underlap for tunneling (squares) and near-thermionic emission (circles). If current is observed in the device with a gate underlap of 1 μm, it means that thermionic emission is dominant since tunneling would be impractical.

local bottom-gate MoS_2 TFT is negligibly small and ohmic contact has been achieved.

Figure 4a shows how transfer characteristics of the local bottom-gate MoS_2 TFT are influenced by incident light for the various power densities (P_{inc}) from 2 to 64 mW cm^{-2} at a wavelength of 532 nm and drain voltage of 1 V. Under the illumination of light at 64 mW cm^{-2}, the current has been increased by 3 orders of magnitude in the off state and by 2.5 times in the on state, respectively. While photoresponsive characteristics are demonstrated only at the off state in the previous multilayer MoS_2 TFT with a conventional global-gate geometry,[17] our local-gate device shows the significant enhancement of current with light both at on and off states. Figure 4b presents photocurrents ($I_{ph} = I_{ds} - I_{dark}$) as a function of power density at off (V_{gs} = 0 V) and on state (V_{gs} = 8 V). Our device shows the excellent linear response of photocurrent to the logarithmic change of optical power, indicating that the local bottom-gate TFT can be used for sensing photons. We also calculated responsivity, $R = I_{ph}/P_{inc}$, and the maximum value of 342.6 A W^{-1} is obtained at 2 mW cm^{-2} in the on state (Figure 4c). Note that this is remarkably higher by more than 3 orders of magnitude than the previously reported value for multilayer MoS_2 TFTs. The large enhancement of photoresponsivity can be also observed in Figure 4d, where photocurrent is plotted for different optical power densities (open symbols) and dark current is also shown as a reference (dashed line). Unlike the previous multilayer MoS_2 phototransistors, the photocurrent of our device in the on state is as comparably large as the dark current, which is achieved by using the local bottom-gate structure.

To characterize the photoswitching behavior of the local bottom-gate MoS_2 TFT, we measure the time-resolved photoresponse as shown in Figure 4e. The measurement was carried out at V_{gs} = −5 V and V_{ds} = 1 V under 638 nm laser at three different incident power densities (2, 4, and 6 mW cm^{-2}). As the illuminating light is switched on and off at an interval of 20 s (a period of 40 s), photocurrent is generated and recombined in accordance with the illumination. A nearly identical response is observed for multiple cycles, exhibiting the reproducibility and the robustness of our local bottom-gate transistors. Figure 4f shows photocurrent measured during one cycle of light modulation in linear scale. Although an accurate response time is not measurable within our experimental setup, the overall photoswitching characteristics demonstrate the potential of our

© 2015 WILEY-VCH Verlag GmbH & Co. KGaA, Weinheim

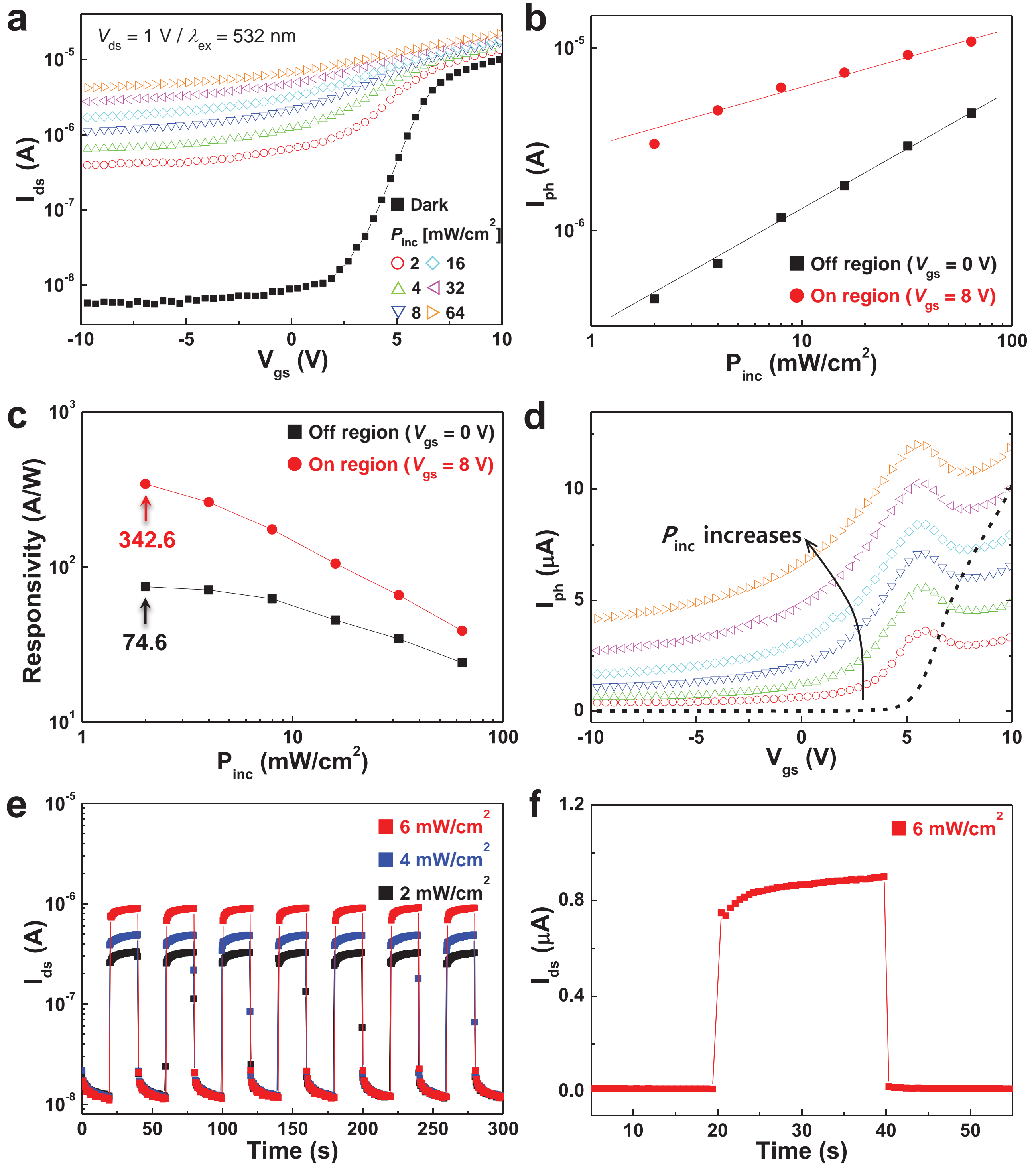

Figure 4. Photoresponsive behavior of a multilayer MoS_2 local bottom-gate phototransistor. a) Comparison of transfer characteristics ($I_{ds} - V_{gs}$) under dark (solid symbol) and light condition (open symbols) with various incident optical power densities (λ_{ex} = 532 nm, P_{inc} = 2, 4, 8, 16, 32, and 64 mW cm^{-2}). b) Photocurrent ($I_{ph} = I_{ds} - I_{dark}$) and c) responsivity as a function of incident power in logarithmic scale, obtained in off (V_{gs} = 0 V) and on (V_{gs} = 8 V) region. d) Photocurrent at various gate voltages for the same conditions of illumination as in Figure 4a (open symbols). Dark current is also shown as a reference (dashed line). (e) Log-scale photoswitching behavior at three different light intensities (2, 4, and 6 mW cm^{-2}) at a wavelength of 638 nm (V_{gs} = −5 V and V_{ds} = 1 V). Photocurrent modulation is induced by the laser, which is switched on and off every 20 s. f) Linear-scale photocurrent in (e) during one cycle of light illumination at 6 mW cm^{-2}.

© 2015 WILEY-VCH Verlag GmbH & Co. KGaA, Weinheim

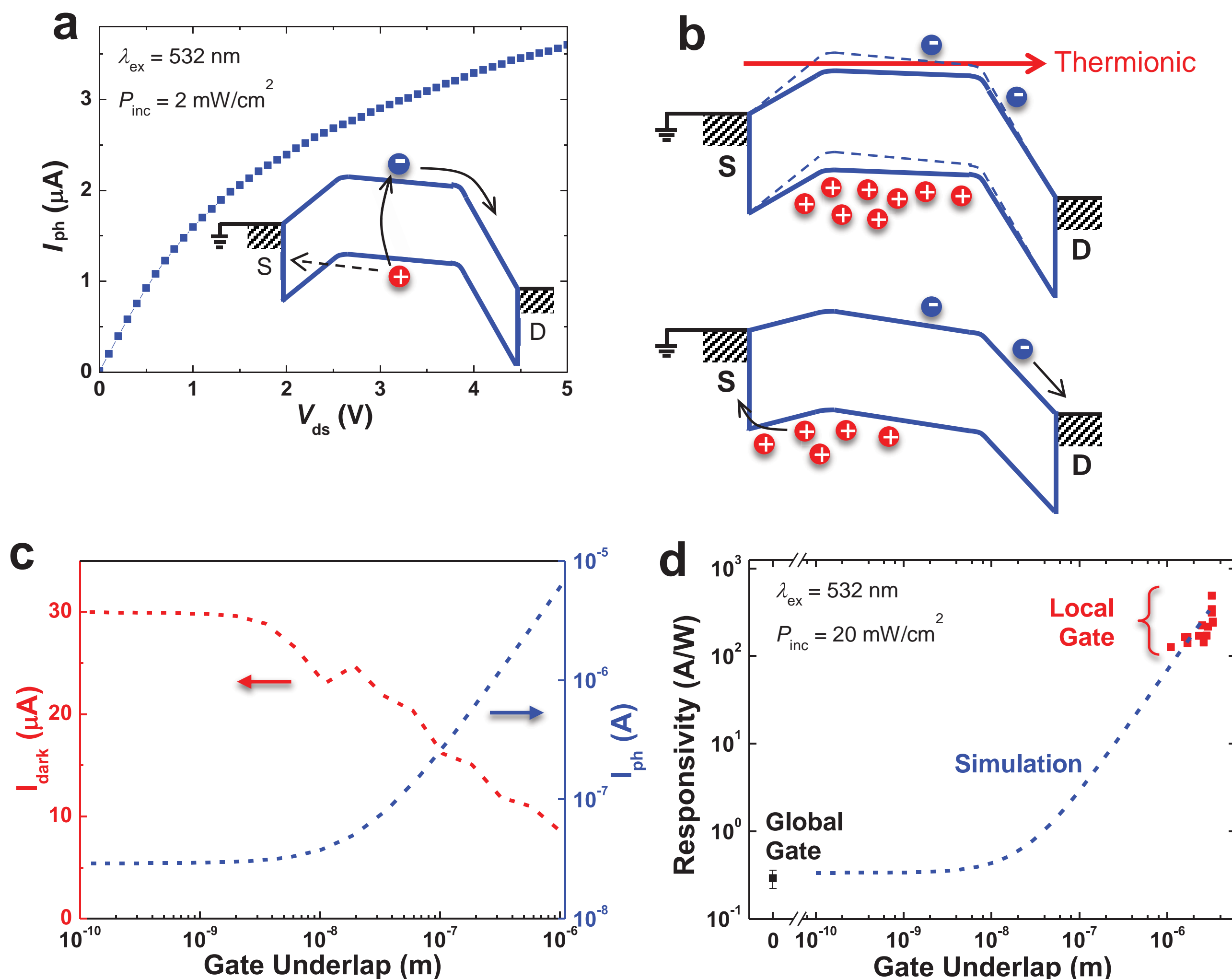

Figure 5. a) Photocurrent at various drain voltages. (Inset) Energy band diagram in the off state. b) (Top) Energy band diagram showing significant accumulation of holes due to the large gate underlap, which reduces the potential barrier for electrons from dashed to solid lines, resulting in the increase of thermionic current. (Bottom) Energy band diagram at an increased gate voltage where the barrier for the hole will become smaller as V_{gs} increases, leading to larger photocurrent. c) Dark current (left axis) and photocurrent (right axis) as a function of gate-underlap length. d) Simulated (blue dashed line) and measured (red squares) photoresponsivity distribution for 14 multilayer MoS_2 phototransistors with various lengths of gate underlap (1.1–3.3 μm). Photoresponsivity distribution for 14 multilayer MoS_2 global-gate phototransistors (black square) shows standard deviation of 25.1% for the normalized responsivity of 0.29 A W^{-1} at a power density of 20 mW cm^{-2}.

local bottom-gate MoS_2 TFTs for highly sensitive photodetector applications.

Next, to understand the photoresponse amplification using the local-gate structure in MoS_2 TFTs, we have plotted photocurrent at 2 mW cm^{-2} at V_{gs} = 0 V (**Figure 5**a), which shows a non-linear behavior to the applied V_{ds}. If the gate underlap is negligibly small or a global-gate structure is used, it would show a linear response to V_{ds} (e.g., see Figure 4c in ref.[17]) following the current equation based on optical absorption as:

$$I_{ph} = 2e\frac{p_{inc}\left(1-e^{-\alpha d}\right)}{h\nu}\tau\mu\frac{W}{L}V_{ds} \tag{2}$$

where e is elementary charge, α and d are absorption coefficient and thickness of multilayer MoS_2, respectively, $h\nu$ is energy of incident photon, τ is average carrier lifetime, and μ is mobility of carriers. However, in our local bottom-gate MoS_2 TFT, such linearity is broken due to the asymmetric barrier in the underlap region as illustrated in the inset of Figure 5a. In particular, holes generated by illuminating light encounter the large tunnel barrier imposed by the gate underlap and they must overcome that large barrier to reach the source (dashed arrow in the inset) whereas electrons can move toward the drain relatively unhampered. Therefore, holes are trapped in the channel region and this local accumulation of holes can reduce the potential barrier for electrons (the top in Figure 5b), resulting in the significant increase of thermionic current even with a relatively small optical power (also see Figure 4a). In fact, I_{ph} of our local-gate MoS_2 TFT in the off state is significantly larger than that of a global-gate structure by more than 2 orders of magnitude for the similar conditions. Moreover, I_{ph} becomes even larger at higher gate voltages (Figure 4d). This is due to the

© 2015 WILEY-VCH Verlag GmbH & Co. KGaA, Weinheim

fact that, as V_{gs} increases, the barrier for the holes will be gradually decreased (as shown in the bottom in Figure 5b). In addition, the dark on current of local-gate TFTs can be smaller than that of global-gate devices for the same channel length due to the series resistance that we have discussed earlier. To sum up, (i) enhanced I_{ph} in the off state, (ii) reduced barriers at larger gate voltages, and (iii) suppressed dark on current are all supportive of photoresponsivity in the on state in our local bottom-gate MoS_2 TFT and, thereby, the large value of 342.6 A W^{-1} could be obtained using our unique device structure.

It might be instructive to investigate how the length of gate underlap affects photoresponsivity in the local-gate MoS_2 TFTs. We have performed comprehensive simulations, which show that, while dark on current can be gradually reduced with gate underlap following Equation (1) (Figure 5c with the left axis), photocurrent will increase significantly as shown in Figure 5c with the right axis. In this simulation, the photocurrent is calculated as:

$$I_{ph} = I_{EHP} + 2I_{off}^{global} \times \exp\left(\frac{e\Delta V_{off}}{mk_B T}\right) \quad (3)$$

where I_{EHP} is the current due to the generation/recombination of electron-hole pairs by illuminating light, I_{off}^{global} is the dark current at off state with global-gate geometry, $e\Delta V_{off}/m$ is the potential energy lowering due to the hole accumulation under the illumination of light, m is the body-effect coefficient, k_B is the Boltzmann constant, T is the temperature, and the factor of 2 comes from our experimental observation to treat the increase of photocurrent in the on state (see Figure 4d) for a fixed optical power. As the gate underlap increases, holes will be accumulated more and the barrier will be reduced, resulting in larger $e\Delta V_{off}$. Photoresponsivity is calculated from this photocurrent at 20 mW cm^{-2} in Figure 5d, which exhibits the trend that the responsivity significantly increases with the gate underlap for the length longer than 10 nm. Statistical distribution of our experimental photoresponsivities for 28 representative multilayer MoS_2 phototransistors is also shown by solid symbols, which is close to the simulation result. Therefore, our experimental data and simulation results provide comprehensive pictures on giant photoamplification in indirect-bandgap multilayer MoS_2 phototransistors based on local bottom-gate multilayer MoS_2 system.

We presented multilayer MoS_2 phototransistors with local bottom-gate structures, in which a gate-controlled region was connected in-series to gate underlap (ungated) regions. Compared with the conventional global bottom-gate structure, our local-gate MoS_2 phototransistor showed outstanding photoresponse. Specifically, the significant enhancement of photocurrent was observed in both on and off states, and the maximum responsivity of 342.6 A W^{-1} was achieved at 2 mW cm^{-2}. Our experiment and simulation revealed that the gate underlap region plays an essential role in enhancing the optoelectronic behavior of indirect-bandgap multilayer MoS_2 phototransistors. We expect that the same strategy can also be applicable to other material systems including monolayer MoS_2 for photoresponsivity amplification through proper engineering of Schottky barrier and gate underlap. The excellent photoresponsive characteristics of our devices suggest that high-gain photodetectors based on multilayer MoS_2 can be realized by engineering optoelectronic device design. Combined with large-area synthesis of MoS_2, the unique architecture in the local bottom-gate multilayer MoS_2 phototransistors can enrich optoelectronic applications such as touch screen panel, image sensor, and communication devices.

Experimental Section

Fabrication: Ti/Au (10/100 nm) for the gate electrode was patterned by conventional photolithography and lift-off process. After patterning the gate electrode, a 100-nm-thick amorphous aluminum oxide (Al_2O_3) of gate insulator was deposited on the substrate through atomic layer deposition with trimethylaluminum (UP Chemical Co. Ltd., South Korea) and H_2O as a precursor and a reactant, respectively.[17] Multilayer MoS_2 for an active channel was mechanically exfoliated from bulk MoS_2 by using a scotch-tape method and transferred onto the gate insulator. In order to form source and drain electrodes, Ti/Au layer was deposited with the thickness of 10/300 nm and patterned. After the fabrication process, the phototransistor was thermally annealed in a vacuum tube furnace with H_2 environment at 200 °C for 2 h to improve the contact resistance.

Physical features of the MoS_2 phototransistor were measured by an optical microscope (BX51M, Olympus Co., Japan) under white light illumination (100 W halogen lamp, U-LH100–3) using bright field imaging modes and 50× objectives. 3D topological image and its line profile data of the MoS_2 phototransistor was investigated by using AFM (XE7 Atomic Force Microscope, Park Systems, South Korea) in the same region as the optical microscope image. The electrical properties of a local bottom-gate MoS_2 phototransistor were investigated by the semiconductor characterization system (Keithley 4200 SCS) with a probe station at room temperature in atmospheric environments.

Simulation: Transmission probability was calculated by using the non-equilibrium Green's function (NEGF) method within the effective mass approximation.[24] Coherent transport is assumed as the length and the width (W/L) are treated in the classical current equation. The effective mass of 0.5 was used for multilayer MoS_2.[25] A Schottky barrier height (Φ_{Bn} = 100 meV) is assumed for tunneling where the transmission probability is calculated at the energy level of 10 meV below the top of the Schottky barrier. The same is also calculated with a relatively small barrier height of 10 meV for near-thermionic emission at the energy level of 10 meV above the chemical potential of the source (μ_s). The energy level of the largest contribution to the current is carefully selected by comparing transmission probability weighted by $(f_1 - f_2)$ where $f_{1,2}$ are the Fermi function at source and drain, respectively. For the ungated channel region, linear potential drop is assumed.[26]

For photocurrent, off current of the global-gate transistor (I_{off}^{global}) is calculated by the current equation for the conventional long-channel devices in the subthreshold region with the following parameters: μ_{eff} = 100 cm^2 V^{-1} s^{-1}, C_{ox} = 6.20 × 10^{-4} F m^{-2}, W = 31.0 µm, L = 11.2 µm at $V_{off} = V_{gs}$ = –1 V (V_{th} = 4.75 V) and V_{ds} = 1 V. The body-effect coefficient of the device is calculated from the measured subthreshold swing (SS) as $m = (SS/2.3) \times (e/k_BT) = 21$. I_{EHP} is treated invariant for different gate voltages at a given optical power and $I_{EHP} = 5000 I_{off}^{global}$ is assumed. The effect of potential barrier lowering is treated by $e\Delta V_{off}/m$ where ΔV_{off} is changed from 0 to 8 V as the length of gate underlap increases from 1 Å to 3 µm.

Acknowledgements

J.K., Y.K.H., G.H., and I.O. contributed equally to this work. This research was supported in part by the National Research Foundation of Korea (Grant Nos. NRF-2013M3C1A3059590, NRF-2014M3A9D7070732, NRF-2013R1A1A2008191, and NRF-2013K1A4A3055679), the Industrial Strategic Technology Development Program (Grant No. 10045145), and

© 2015 WILEY-VCH Verlag GmbH & Co. KGaA, Weinheim

NSERC Discovery Grant (No. RGPIN-05920–2014). G.H. acknowledges the financial support by NSERC Canada Graduate Scholarships Program.

Received: September 22, 2014
Revised: January 13, 2015
Published online: February 13, 2015

[1] Q. H. Wang, K. Kalantar-Zadeh, A. Kis, J. N. Coleman, M. S. Strano, *Nat. Nanotechnol.* **2012**, *7*, 699.
[2] M. Chhowalla, H. S. Shin, G. Eda, L. J. Li, K. P. Loh, H. Zhang, *Nat. Chem.* **2013**, *5*, 263.
[3] M. Xu, T. Liang, M. Shi, H. Chen, *Chem. Rev.* **2013**, *113*, 3766.
[4] A. K. Geim, I. V. Grigorieva, *Nature* **2013**, *499*, 419.
[5] X. Huang, Z. Zeng, H. Zhang, *Chem. Soc. Rev.* **2013**, *42*, 1934.
[6] D. Jariwala, V. K. Sangwan, L. J. Lauhon, T. J. Marks, M. C. Hersam, *ACS Nano* **2014**, *8*, 1102.
[7] R. Ganatra, Q. Zhang, *ACS Nano* **2014**, *8*, 4074.
[8] H. Li, J. Wu, Z. Yin, H. Zhang, *Acc. Chem. Res.* **2014**, *47*, 1067.
[9] X. Huang, C. Tan, Z. Yin, H. Zhang, *Adv. Mater.* **2014**, *26*, 2185.
[10] B. Radisavljevic, A. Radenovic, J. Brivio, V. Giacometti, A. Kis, *Nat. Nanotechnol.* **2011**, *6*, 147.
[11] S. Kim, A. Konar, W. S. Hwang, J. H. Lee, J. Lee, J. Yang, C. Jung, H. Kim, J. B. Yoo, J. Y. Choi, Y. W. Jin, S. Y. Lee, D. Jena, W. Choi, K. Kim, *Nat. Commun.* **2012**, *3*, 1011.
[12] B. Radisavljevic, A. Kis, *Nat. Mater.* **2013**, *12*, 815.
[13] H. Liu, P. D. Ye, *IEEE Electron Device Lett.* **2012**, *33*, 546.
[14] L. Liu, Y. Lu, J. Guo, *IEEE Trans. Electron Devices* **2013**, *60*, 4133.
[15] S. Das, H. Y. Chen, A. V. Penumatcha, J. Appenzeller, *Nano Lett.* **2013**, *13*, 100.
[16] Z. Yin, H. Li, H. Li, L. Jiang, Y. Shi, Y. Sun, G. Lu, Q. Zhang, X. Chen, H. Zhang, *ACS Nano* **2012**, *6*, 74.
[17] W. Choi, M. Y. Cho, A. Konar, J. H. Lee, G. B. Cha, S. C. Hong, S. Kim, J. Kim, D. Jena, J. Joo, S. Kim, *Adv. Mater.* **2012**, *24*, 5832.
[18] O. Lopez-Sanchez, D. Lembke, M. Kayci, A. Radenovic, A. Kis, *Nat. Nanotechnol.* **2013**, *8*, 497.
[19] W. Zhang, J. K. Huang, C. H. Chen, Y. H. Chang, Y. J. Cheng, L. J. Li, *Adv. Mater.* **2013**, *25*, 3456.
[20] F. Xia, T. Mueller, R. Golizadeh-Mojarad, M. Freitag, Y.-M. Lin, J. Tsang, V. Perebeinos, P. Avouris, *Nano Lett.* **2009**, *9*, 1039.
[21] M. R. Esmaeili-Rad, S. Salahuddin, *Sci. Rep.* **2013**, *3*, 2345.
[22] W. Zhang, C.-P. Chuu, J.-K. Huang, C.-H. Chen, M.-L. Tsai, Y.-H. Chang, C.-T. Liang, Y.-Z. Chen, Y.-L. Chueh, J.-H. He, *Sci. Rep.* **2014**, *4*, 3826.
[23] H. Xu, J. Wu, Q. Feng, N. Mao, C. Wang, J. Zhang, *Small* **2014**, *10*, 2300.
[24] S. Datta, *Quantum Transport: Atom to Transistor*, Cambridge University Press, New York **2005**.
[25] V. Mishra, S. Smith, K. Ganapathi, S. Salahuddin, *IEEE IEDM Tech. Dig.* **2013**, 136.
[26] Y. Yoon, J. Fodor, J. Guo, *IEEE Trans. Electron Devices* **2008**, *55*, 283.

© 2015 WILEY-VCH Verlag GmbH & Co. KGaA, Weinheim